HHS Public Access

Author manuscript

Dev Biol. Author manuscript; available in PMC 2019 November 15.

Published in final edited form as:

Dev Biol. 2018 November 15; 443(2): 153–164. doi:10.1016/j.ydbio.2018.09.011.

A spontaneous mouse deletion in *Mctp1* uncovers a long-range cis-regulatory region crucial for NR2F1 function during inner ear development

Basile Tarchini[a,b,c], **Chantal Longo-Guess**[a], **Cong Tian**[a,c], **Abigail L.D. Tadenev**[a], **Nicholas Devanney**[a], and **Kenneth R. Johnson**[a]

[a]The Jackson Laboratory, Bar Harbor, ME, 04609, USA

[b]Department of Medicine, Tufts University, Boston, 02111, MA, USA

[c]Graduate School of Biomedical Science and Engineering (GSBSE), University of Maine, Orono, 04469, ME, USA

Abstract

Hundreds of thousands of cis-regulatory DNA sequences are predicted in vertebrate genomes, but unlike genes themselves, few have been characterized at the functional level or even unambiguously paired with a target gene. Here we serendipitously identified and started investigating the first reported long-range regulatory region for the *Nr2f1 (Coup-TFI)* transcription factor gene. NR2F1 is temporally and spatially regulated during development and required for patterning and regionalization in the nervous system, including sensory hair cell organization in the auditory epithelium of the cochlea. Analyzing the deaf wanderer (*dwnd*) spontaneous mouse mutation, we traced back the cause of its associated circling behavior to a 53 kb deletion removing five exons and adjacent intronic regions of the poorly characterized *Mctp1* gene. Interestingly, loss of *Mctp1* function cannot account for the hearing loss, inner ear dysmorphology and sensory hair cell disorganization observed in *dwnd* mutants. Instead, we found that the $Mctp1^{dwnd}$ deletion affects the *Nr2f1* gene located 1.4 Mb away, downregulating transcription and protein expression in the embryonic cochlea. Remarkably, the $Mctp1^{dwnd}$ allele failed to complement a targeted inactivation allele of *Nr2f1*, and transheterozygotes or $Mctp1^{dwnd}$ homozygotes exhibit the same morphological defects observed in inner ears of *Nr2f1* mutants without sharing their early life lethality. Defects include improper separation of the utricle and saccule in the vestibule not described previously, which can explain the circling behavior that first brought the spontaneous mutation to attention. By contrast, mice homozygous for a targeted inactivation of *Mctp1* have normal hearing and inner ear structures. We conclude that the 53 kb $Mctp1^{dwnd}$ deletion encompasses a long-range cis-regulatory region essential for proper *Nr2f1* expression in the embryonic inner ear, providing a first opportunity to investigate *Nr2f1* function in postnatal inner

Correspondence to: Basile Tarchini; Kenneth R. Johnson.

ears. This work adds to the short list of long-range regulatory regions characterized as essential to drive expression of key developmental control genes.

Keywords

deafness; inner ear development; cis-regulation; long-range enhancer; *Mctp1*; *Nr2f1*

1. Introduction

Nuclear receptor subfamily 2, group F, members 1 and 2 (NR2F1 and NR2F2, also known as COUP-TFI and COUP-TFII) are well-characterized orphan nuclear receptors belonging to the superfamily of steroid/thyroid hormone receptors. They function as ligand-related transcription factors that can both activate and repress target gene expression. Their evolutionarily conserved DNA sequences and the early lethality associated with their loss-of-function mutations suggest that they play vital roles in many developmental processes (Pereira et al., 2000). Most mice that are homozygous for a null mutation of *Nr2f1* die perinatally, with only a few surviving until 3-4 weeks of age. The mutant mice exhibit defects of neuronal differentiation and axon guidance (Armentano et al., 2006; Qiu et al., 1997; Yamaguchi et al., 2004; Zhou et al., 1999), irregularities in the patterning and regionalization of the neocortex (Armentano et al., 2007; Bertacchi et al., 2018; Zhou et al., 2001), and inner ear abnormalities (Tang et al., 2006).

Nr2f1 expression is spatially and temporally regulated during mouse development, suggesting that it may be involved in tissue-specific organogenesis. *Nr2f1* is highly expressed in the nervous system, especially in organs that develop by epithelial proliferation and differentiation like the ectoderm of the inner ear (Pereira et al., 2000). *Nr2f1* is expressed early in the development of the otic vesicle and later in the developing cochlear duct and maturation of the organ of Corti (Tang et al., 2005). Inner ears of developing *Nr2f1*-null mice exhibit a short cochlear duct with supernumerary hair cells in the apical turn, which led the authors to suggest that *Nr2f1* may control Notch regulation of cochlear hair cell differentiation (Tang et al., 2006). Human clinical studies also support a role for NR2F1 in cochlear development and function. A patient with a paracentric chromosomal inversion accompanied by a deletion of *Nr2f1* exhibited syndromic deafness (Brown et al., 2009), and 20% of individuals with pathogenic *Nr2f1* variants were shown to have associated hearing defects (Chen et al., 2016). *Nr2f1* (COUP-TFI) mutations underlie autosomal-dominant Bosch-Boontra-Schaaf optic atrophy syndrome (BBSOAS), which is characterized by delayed development, intellectual disability, and optic atrophy (OMIM #615722). Clinical features may also include hypotonia, seizures, autism spectrum disorder, oromotor dysfunction, thinning of the corpus callosum, and hearing defects (Bosch et al., 2014; Chen et al., 2016).

Although NR2F1 has been extensively studied and many of its transcriptional targets have been identified (Montemayor et al., 2010; Pereira et al., 2000), the mechanisms that underlie its own spatial and temporal expression patterns are largely unknown. Distally located cis-regulatory elements (enhancers) can function at large distances from their target genes and

are key contributors to the spatiotemporal expression patterns of transcription factors that guide morphogenesis during development (Bulger and Groudine, 2011; Long et al., 2016; Ong and Corces, 2011; Shlyueva et al., 2014). Advances in DNA sequencing have led to estimates of hundreds of thousands of enhancers in the vertebrate genome, but few have been identified with known target genes or phenotypic consequences, and these usually involve the dysregulation of key developmental control genes (Kleinjan and van Heyningen, 2005; Spitz, 2016). Although *Nr2f1* is an important developmental control gene, no long-range regulators have yet been identified that modulate its expression or that are associated with any of its disease phenotypes (Zhang et al., 2018).

Here, we report on the discovery of a long-range regulator of *Nr2f1* expression with specific effects on inner ear development in the mouse. We identified a new spontaneous mouse mutation, named “deaf wanderer” (symbol *dwnd*), by its associated hearing and balance deficits and found that it is a 53 kb deletion within the *Mctp1* gene, but that *Mctp1* dysfunction is not responsible for its mutant phenotype. Because the inner ear abnormalities of $Mctp1^{dwnd/dwnd}$ mutant mice are very similar to those reported in mice homozygous for a null mutation of the nearby *Nr2f1* gene (Tang et al., 2006), we hypothesized and later confirmed that the loss of cis-regulatory sequences located in the deleted region of the $Mctp1^{dwnd}$ allele severely reduces *Nr2f1* expression in the inner ear and disrupts its development. The mammalian inner ear is a very complex and intricate structure that requires a highly coordinated pattern of cell-type and stage-specific transcriptional regulation for its development (Doetzlhofer and Avraham, 2017; Fritzsch et al., 2015; Groves and Fekete, 2012; Wu and Kelley, 2012). Our discovery of a critical regulatory region for *Nr2f1* within the *Mctp1* gene adds to our understanding of how such a precise patterning of gene expression is achieved.

2. Materials and methods

2.1. Mice

All mice in this study were obtained from research or production colonies and housed in the Research Animal Facility at The Jackson Laboratory (JAX) in Bar Harbor, ME. JAX is accredited by the American Association for the Accreditation of Laboratory Animal Care. All procedures involving the use of mice were approved by the JAX Institutional Animal Care and Use Committee and were performed in accordance with the guidelines and regulations of the US National Institutes of Health Office of Laboratory Animal Welfare and the Public Health Service Policy on the Humane Care and Use of Laboratory Animals.

The recessive *dwnd* mutation occurred spontaneously in the C57BL/10SnJ colony of mice at The Jackson Laboratory (JAX) and was shown to be an intragenic deletion of the *Mctp1* gene. To alleviate breeding problems, a congenic inbred strain was developed by repeated backcrossing of mutant mice to the C57BL/6J inbred strain until achieving the equivalent of 6 backcross generations, followed by inbreeding to generate the B6.B10Sn-$Mctp1^{dwnd}$/Kjn congenic strain, which is homozygous for the $Mctp1^{dwnd}$ allele and available from JAX as Stock # 9690. All studies of the $Mctp1^{dwnd}$ mutation described here were done with mice of this congenic strain. Homozygous mutant mice ($Mcpt1^{dwnd/dwnd}$) can sometimes be

identified by their moderate circling behavior, but penetrance of this phenotype is only about 35% compared with full penetrance of elevated ABR thresholds.

Three additional mouse strains were used in this study. The B6N(Cg)-*Nr2f1*$^{tm1.1(KOMP)Mbp}$/J strain with a knockout mutation of the *Nr2f1* gene was generated by the Knockout Mouse Phenotyping Program (KOMP^2) at The Jackson Laboratory. Cryopreserved sperm from the C57BL/6NCrl *Mctp1*$^{em1(IMPC)Mbp}$/Mmucd strain was imported from the Mutant Mouse Resource & Research Center (MMRC) at the University of California, Davis, and mice were recovered for research use at The Jackson Laboratory. The B6.129-*Lhfpl5*^{tm1Kjn}/Kjn strain (JAX Stock # 5434) contains a *LacZ* reporter gene in the *Lhfpl5* gene that is expressed specifically in hair cells of the inner ear (Longo-Guess et al., 2007).

Embryonic stages of mice were determined from timed matings by observing females for vaginal plugs. The day of the plug was considered embryonic day 0.5 (E0.5).

2.2. ABR measurements

Hearing in mice was assessed by ABR threshold analysis. Mice were anesthetized with an intraperitoneal injection of tribromoethanol (0.2 ml of 20 mg/ml stock per 10 g of body weight), and then placed on a 37°C temperature-controlled pad (FHC Inc., Bowdoin, ME) in a soundattenuating chamber (Acoustic Systems, Austin, TX). Needle electrodes were placed just under the skin, with the active electrode placed between the ears just above the vertex of the skull, the ground electrode placed ventrolateral to the right ear, and the reference electrode underneath the left ear. High-frequency transducers were placed just inside the ear canal and computer-generated sound stimuli were presented at defined intervals. Thresholds were determined for broad-band clicks and 8-, 16-, and 32-kHz pure-tone stimuli by increasing the sound pressure level (SPL) in 10-dB increments followed by 5-dB increases and decreases to determine the lowest level at which a distinct ABR wave pattern could be recognized. Stimulus presentation and data acquisition were performed using the Smart EP evoked potential system (Intelligent Hearing Systems, Miami, FL).

2.3. Inner ear whole mounts and X-gal staining of hair cells

To better visualize cochlear lengths in whole mount preparations, we crossed B6.B10Sn-*Mctp1*^{dwnd}/J mice with mice of the B6.129-*Lhfpl5*^{tm1Kjn}/Kjn knockout strain, which contains a *LacZ* reporter gene for *Lhfpl5* that is expressed specifically in hair cells of the inner ear (Longo-Guess et al., 2007). *Lhfpl5*$^{+/-}$ and *Mctp1*$^{+/dwnd}$ doubly heterozygous mice were intercrossed, and *Mctp1*$^{+/+}$ and *Mctp1*$^{dwnd/dwnd}$ progeny with *Lhfpl5*$^{+/-}$ genotypes were selected for cochlear hair cell visualization by X-gal detection of the *LacZ* reporter gene for *Lhfpl5* expression, performed essentially as described (Oberdick J, 1994). Briefly, inner ears were dissected from the mouse and fixed overnight in 2% PFA in 0.1M modified PIPES buffer. After fixation, the bony shell of the cochlea was removed and the inner ears were stained overnight at 37°C in X-gal buffer. Whole mount inner ears were visualized using a Leica MZ12.5 stereomicroscope and Leica Application Suite software v3.6.0 (Leica Microsystems GmbH, Wetzlar, Germany).

2.4. Scanning electron microscopy of cochlear hair cells

SEM was performed essentially as described (Furness and Hackney, 1986). Inner ears were dissected out of the skull, fixed in 2.5% glutaraldehyde in 0.1 M cacodylate buffer for 3-4 h at 4°C, and then washed three to four times in 0.1 M phosphate buffer. Hair cells of the organ of Corti were exposed by carefully dissecting away the overlying bone and membranes. The tissues were then processed in osmium tetroxide-thiocarbohydrazide (OTOTO), dehydrated with ethanol, and dried with hexamethyldisilazane (Electron Microscopy Sciences, Hatfield, PA). Samples were mounted onto aluminum stubs, sputter-coated to produce a 15-nm gold coat, and examined at 20 kV with a Hitachi 3000N VP Scanning Electron Microscope with an EDAX X-ray Microanalysis unit and PCI Quartz Image Management software (Vancouver, BC).

2.5. Hair cell counts and measurements of cochlear length

Hair cell counts and cochlear lengths were determined from rhodamine phalloidin stained surface preparations of P0 cochlea. After staining, each of the three turns: apical, middle, and basal were separated from the modiolus, mounted onto glass slides, and imaged with an Olympus BX51 microscope and a DP72 camera with cellSens standard software (Olympus, Tokyo, Japan). Cochlear measurements were taken using the same software. Inner and outer hair cells were counted separately from three random sections of each turn of an individual cochlea. Hair cell density per 100 μm was calculated for each of the two hair cell populations. Lengths for each of the three sections of the cochlear duct were measured from digital images of the phalloidin preps, and these partial lengths were added together to give a total cochlear length for each ear.

2.6. Immunofluorescence and phalloidin stainings

E16.5 inner ears or eyes were fixed for 1 hour in PFA 4%, equilibrated in sucrose 20% overnight and embedded in a 1:1 mixture of sucrose 20%: OCT (Tissue-Tek). Cryosections (12μm) were stored at −80C, thawed, and processed for citrate antigen retrieval (boiled five times for 1 minute in 10mM citrate with cooling intervals). The sections were then permeabilized and blocked in 0.5% Triton X-100 and 1% BSA, and incubated with the primary antibodies overnight (NR2F1: R&D Systems PPH813299, mouse monoclonal clone H8132 (1:100); SOX2: Santa Cruz Biotechnology sc-17320, goat polyclonal (1:100)). Secondary antibodies were donkey anti-mouse conjugated to Alex Fluor 555 and donkey anti-goat conjugated to Alex Fluor 647 (Thermofisher). Nuclei were stained with Hoechst 33342 (Thermofisher). For the quantifications in Fig. 3D, a 25×25 μm region of interest was defined to match the organ of Corti, and signal intensity was measured separately for the SOX2 and NR2F1 channels using ImageJ (IntDens). For whole-mounts at birth (Fig. 5), inner ears were fixed 1 hour in 4% PFA, the sensory epithelia were exposed, permeabilized in 0.5% Triton X-100, stained with phalloidin conjugated to Alexa Fluor 488 (Thermofisher), and mounted flat. Images were acquired with a Zeiss LSM800 confocal microscope.

2.7. Inner ear paint fills

E15.5 embryos (*Mctp1*$^{dwnd/dwnd}$, n = 4; *Mctp1*$^{-/-}$, n = 3; *Nr2f1*$^{-/-}$, n = 4; *Mctp1*$^{+/dwnd}$ *Nr2f1*$^{-/-}$, *n* = 5; and *Mctp1*$^{+/dwnd}$, *n* = 6) and P1 mice (*Mctp1*$^{dwnd/dwnd}$, *n* = 3; *Mctp1*$^{+/dwnd}$, *n* = 3) were used for inner ear paint fills. E15.5 embryos were decapitated and whole heads were fixed in Bodian's fixative. P1 mice were decapitated and half-heads were fixed in Bodian's fixative after the brain was removed. Heads were fixed overnight and then dehydrated with 75% ethanol (2 × 2 h), 95% ethanol (2 × 2 h), and 100% ethanol (2 × 2 h). Heads were then rinsed once with methyl salicylate and cleared overnight by placing specimens in methyl salicylate. Inner ears were filled with 1% Wite-Out correction fluid in methyl salicylate using a Hamilton syringe with a pulled glass capillary needle broken to a tip diameter of 20–40 μm. E15.5 inner ears were injected through the middle turn of the cochlea. Two injections were done for P1 inner ears with one injection in the cochlear middle turn and the second injection in the common crus, as previously described (Kiernan, 2006; Tian et al., 2017).

2.8. PCR methods for mutation analysis and genotyping

DNA samples from backcross progeny were isolated from mouse tail tips using the hot sodium hydroxide and Tris (HotSHOT) method (Truett et al., 2000). For linkage mapping, microsatellite markers were selected for each chromosome, genotyped by PCR using the HotMaster Taq DNA Polymerase kit (5 PRIME Inc., Gaithersburg, MD) according to manufacturer's instructions, and analyzed for cosegregation with the mutant phenotype, which was assessed by ABR.

PCR primers for sequencing *Mctp1* exons and to genotype mice for *Mctp1*^{dwnd} mutation were designed using Primer3 software (http://primer3.ut.ee) and synthesized by Integrated DNA Technologies (Coralville, Iowa). Pairs of primers flanking each of the 21 exons of *Mctp1* were used to amplify and sequence DNA products from *dwnd/dwnd* and +/+ mice. Three primers were used in a single PCR reaction to distinguish +/+, +/*dwnd* and *dwnd/dwnd* genotypes of mice from genomic DNA: a forward primer located outside the deletion (`ACAGGAGGTCAGGGTGTGTC`), a forward primer located within the deletion (`TGCCAAAGAGCATTAGTGTGAT`), and a reverse primer located outside the deletion (`TTCTCACTGGTTTCACACCATC`), as indicated in Fig. 2A. PCR products were separated on 3% NuSieve gels (Lonza, Rockland, ME) containing ethidium bromide and visualized by UV illumination.

2.9. RT-qPCR

Whole cochleae of E16.5 embryos were microdissected from the condensed mesenchyme shell and flash frozen in liquid nitrogen. Following genotyping of the litter, samples of the same genotype (heterozygous or homozygous for *Mctp1*^{dwnd}) were pooled and RNA extracted using the RNeasy Plus mini kit (Qiagen). Two litters were processed in this way, with each genotype group containing between 6-10 cochleae per litter. RNA was then reverse-transcribed using an oligo-dT primer to obtain first-strand cDNA using standard methods, and qPCR performed using a SYBR Green PCR Master Mix (ThermoFisher #4309155) and a ViiA 7 Real-Time PCR System (ThermoFisher). Primers used were as follows: GAPDH F: `AGGTCGGT GT GAACGGATTT G`, GAPDH R:

TGTAGACCATGTAGTTGAGGTCA, Nr2f1 F: CGAGTACAGCTGCCTCAAAG (exon 2), Nr2f1 R: CTTTCGATGTGGGCAGCATC (exon 3), Mctpl F: GCTGATCCCGGAATGTACCA (exon2/first coding), Mctp1 R: CACATACGGATCGCTTGTCC (exon 3). Reactions were run in triplicate and fold changes for target transcripts versus the *Gapdh* housekeeping gene were calculated using the ΔΔCt method (Livak and Schmittgen, 2001) on the averaged Ct values from the triplicate reactions. Data points represent the samples pooled by genotype for each of the two litters collected.

3. Results

3.1. The phenotype of dwnd/dwnd mutant mice

A new recessive mutation was discovered at The Jackson Laboratory, first identified by the moderate circling behavior of homozygous individuals. Because circling behavior is characteristic of inner ear vestibular dysfunction, mutant mice were evaluated for hearing acuity by auditory brainstem response (ABR) measurements and found to be hearing impaired, with ABR thresholds 25-45 dB above those of age-matched control mice (Fig. 1A). The new mutation was named “deaf wanderer” (symbol *dwnd*) because of its associated auditory and vestibular dysfunctions. From intercrosses of obligate +/*dwnd* mice, we deduced that hearing impairment, which occurred in about 25% of the progeny, was fully penetrant in *dwnd/dwnd* mice, but that only about 40% of the hearing-impaired *dwnd/dwnd* progeny exhibited circling behavior.

To search for cochlear abnormalities that may be responsible for the hearing impairment of mutant mice (*dwnd/dwnd*), we compared scanning electron microscopy (SEM) images of organ of Corti surface preparations from cochleae of mutant and control mice (Fig. 1B-E). Compared with +/+ controls (Fig. 1B,D), the cochleae of *dwnd/dwnd* mice have additional, disorganized inner hair cells (IHCs) near the base (Fig. 1C) and an extra row of outer hair cells (OHCs) near the apex (Fig. 1E). Cross-sectional analysis by light microscopy revealed no additional cochlear abnormalities; however, examinations of dissected and cleared whole-mounts of inner ears showed that the cochlea of *dwnd/dwnd* mice is smaller and shorter than that of +/+ controls (Fig. 1F). For better visualization of the cochlear duct, whole mounts were stained with X-gal to detect expression of a hair cell-specific *Lhfpl5-LacZ* reporter gene, as detailed in Materials and Methods.

To examine global inner ear morphology, paintfills of inner ears from newborn *dwnd/dwnd* mice were compared with those of +/+ controls (Fig. 1G). The cochlear duct of *dwnd/dwnd* mice appeared shorter than controls, as seen in the whole mount inner ear preparations (Fig. 1F); however, additional abnormalities were revealed in other inner ear structures. The saccule of the mutant inner ear is noticeably smaller than that of the control and is not fully separated from the utricle, and the duct connecting the saccule with the cochlea is much larger in the mutant (Fig. 1G).

Hair cell counts and cochlear length measurements in mutant and control mice supported the histological observations. The cochleae of *dwnd/dwnd* mutants have a greater density of IHCs near the apex and near the base (Fig. 1H), a much greater OHC density near the apex (Fig. 1I), and a shorter length (Fig. 1J) compared with cochleae of +/+ controls. Although

hair cell densities are greater in *dwnd/dwnd* mutants than controls, the shorter cochlear length suggests that the total number of hair cells is similar.

3.2. Genetic mapping of the dwnd mutation

The chromosomal map position of the *dwnd* mutation was determined by genetic analysis of 159 progeny from a (B6.B10Sn-*dwnd/dwnd* × C3HeB/FeJ) F1 × B6.B10Sn-*dwnd/dwnd* backcross. Because of the incomplete penetrance of circling behavior, each of the backcross mice was assigned a genotype (*dwnd/dwnd* or +/*dwnd*) according to its ABR thresholds (Fig. 1A). Genotypes of mice were analyzed for co-segregation with polymorphic microsatellite markers located throughout the genome, and linkage was found with markers on Chromosome 13 in a region between markers *D13Mit26* (72.2 Mb) and *D13Mit193* (91.8 Mb), GRCm38 Mb positions. This 20 Mb region contains more than 60 protein-coding genes, but only three are known to affect inner ear development or function: *Nr2f1*, *Adgrvl*, and *Slcl2a7*, according to the Mouse Genome Informatics website (http://www.informatics.jax.org/marker) results for this region using “inner ear” as the phenotype search term.

The *Nr2f1* gene stood out as a likely candidate because a mouse knockout of this gene (Tang et al., 2006) has an inner ear phenotype that is very similar to what we observed for *dwnd/dwnd* mice. However, we initially eliminated *Nr2f1* as a candidate gene because genomic DNA from *dwnd/dwnd* mutants and +/+ control mice showed no sequence differences in any of the *Nr2f1* exons or their adjacent splice sites. Although *Slcl2a7*$^{-/-}$ and *Adgrvl*$^{-/-}$ mice are deaf, their inner ear phenotypes are very distinct from that of *dwnd/dwnd* mice; neither has supernumerary cochlear hair cells nor exhibits behaviors characteristic of vestibular dysfunction. *Slcl2a7*$^{-/}$ mutant mice exhibit rapid outer hair cell degeneration but have no other inner ear abnormalities (Boettger et al., 2002), and inner ear defects of *Adgrvl*$^{-/}$ mice are limited to disorganized stereocilia bundles of cochlear hair cells (McGee et al., 2006). Because of their distinctively different mutant phenotypes, *Slc12a7* and *Adgrvl* were not further considered as candidate genes for the *dwnd* mutation.

Information on each of the remaining genes in the *dwnd* candidate interval was accessed from the Mouse Genome Database (http://www.informatics.jax.org/marker), but none of the well-characterized genes in the interval have functions or expression patterns that we deemed relevant to inner ear development. Of the poorly characterized genes, we selected *Mctp1* as a possible candidate because of its proposed function in calcium signaling at the plasma membrane (Shin et al., 2005), which we thought could relate to the defect in cochlear convergent extension observed in *dwnd* mutant mice (Fig. 1), a process that involves intercellular calcium signaling. *Mctp1* spans more than 540 kb and is comprised of 21 exons (Fig. 2A), which encode a 694 amino acid protein containing three C2 calcium-binding domains and two transmembrane helices (Shin et al., 2005), as shown in Fig. 2B. The presence of multiple C2 domains suggested to us that MCTP1 might function as a Ca^{2+} sensor in membranes of the inner ear similar to otoferlin, a multi-C2 domain protein that is essential for hearing (Pangrsic et al., 2012). In addition, transcriptome analyses using mouse expression arrays (Hertzano et al., 2011) and RNA-seq (Maass et al., 2016) suggested that *Mctp1* is expressed in auditory sensory cells of P0-P6 mice. For these reasons and because

no associated phenotypes had been reported for *Mctp1* mutations, we investigated the possibility that *Mctp1* dysfunction may underlie the *dwnd/dwnd* phenotype.

3.3. Molecular analysis of the Mctp1 candidate gene

To evaluate the *Mctp1* candidate gene, three sets of PCR primers were designed to amplify overlapping cDNA products (reference sequence NM_030174). Using primers located in exons 9 and 17, a much smaller 491 bp product was amplified from *dwnd* cDNA as compared to the 994 bp product amplified from the control cDNA (Fig. 2C). Sequencing of the smaller product showed that *dwnd* cDNA is missing exons 11-15 of the *Mctp1* transcript (Fig. 2B). No size differences were observed for products amplified with the other *Mctp1* cDNA primer sets. The *dwnd* deletion is predicted to cause a frameshift and premature stop codon at the beginning of exon 16 and therefore is expected to eliminate the third C2 domain and the two transmembrane helices of the MCTP1 protein, thus inactivating normal MCTP1 function (Fig. 2B).

To confirm the *dwnd* mutation at the genomic level, primers specific to each of the 21 *Mctp1* exons were used to amplify and sequence products from mutant and control DNA. The primers for exons 11-15 did not amplify any products when *dwnd/dwnd* DNA was used as the template, but all other primer sets produced the expected wildtype product sizes with no sequence differences between mutant and control DNA. The extent of the *dwnd* deletion was refined by PCR analysis using multiple primer pairs distributed throughout intron 10-11 and intron 15-16. The presence or absence of the PCR products further delimited the boundaries of the deleted region. Sequencing of genomic DNA of *dwnd/dwnd* mice amplified with primers flanking the deletion showed that 53,008 bp are precisely deleted without any accompanying DNA alterations. In addition to the 4830 bp that includes exons 11-15 and the introns between these exons, the deletion includes 7270 bp of flanking intron 10-11 and 40,908 bp of flanking intron 15-16.

To distinguish between the genotypes of *dwnd/dwnd*, +/*dwnd*, and +/+ mice, a three-primer genotyping assay was devised using a common reverse primer located outside of the deletion and a forward primer that spans across the deletion (to amplify the mutant product) combined with a forward primer located within the deletion (to amplify the wildtype product), as shown in Fig. 2A. A 450 bp product was obtained from DNA of wild type mice, and a 375 bp band was obtained in *dwnd/dwnd* mice, with heterozygotes (+/*dwnd*) exhibiting both bands (Fig. 2D). The *Mctp1* genotypes obtained from DNA analysis corresponded with wildtype (+/+ and +/*dwnd*) and mutant (*dwnd/dwnd*) phenotypes of all mice examined in this study, supporting the causative nature of the $Mctp1^{dwnd}$ mutation. Because the spontaneous *dwnd* mutation arose recently in the C57BL/10SnJ inbred mouse strain, it is expected to be the only DNA difference between the C57BL/10SnJ strain and the congenic region of the *dwnd* mutant strain (B6.B10Sn-$Mctp1^{dwnd}$/Kjn, see Materials and Methods), providing further confirmation that the *Mctp1* intragenic deletion we discovered, and not some other undetected mutation, is responsible for the *dwnd/dwnd* phenotype.

3.4. Nr2f1 transcript and protein are downregulated in the Mctp1$^{dwnd/dwnd}$ cochlea

We could not localize or quantitate *Mctp1* expression in the embryonic cochlea because, in our hands, *in situ* hybridization and immunohistochemistry revealed only faint *Mctp1* transcript and protein signals close to background levels. The site of *Mctp1*^{dwnd} deletion at the 76.8 Mb position on mouse Chromosome 13 is 1.4 Mb from the *Nr2f1* gene at the 78.2 Mb position (Fig. 2E). Four intervening genes separate *Mctp1* from *Nr2f1* (*Pou5f2, Fam172a, 2210408121Rik, Slf1*) and no distant regulatory sequence for *Nr2f1* has been reported so far. Relative physical proximity and the similarities in the inner ear abnormalities of *Mctp1*$^{dwnd/dwnd}$ (Fig. 1) and *Nr2f1*$^{-/}$ (Tang et al., 2006) mice nevertheless prompted us to test whether the *Mctp1*$^{dwnd/dwnd}$ mutant phenotype could be caused by the loss of *cis*-regulatory elements for *Nr2f1* transcription located in the *Mctp1*^{dwnd} deletion, and not by the loss of MCTP1 function itself. To compare transcript levels, the membranous labyrinths of E16.5 cochlea from +/*dwnd* and *dwnd/dwnd* fetuses were pooled by genotype, cDNA prepared and RT-qPCR performed with primer pairs for *Mctp1* (exon 2-3) and *Nr2f1* (exon 2-3). Fold change calculated using the ΔΔCt method revealed that *Mctp1* expression was reduced ~75% in the *Mctp1*$^{dwnd/dwnd}$ cochlea, indicating that truncated transcripts are less stable than wildtype (Fig. 3A), an unsurprising finding because the premature stop codon is likely to activate nonsense-mediated decay of the mutant transcript. In comparison, *Nr2f1* expression was reduced ~50% in the *Mctp1*$^{dwnd/dwnd}$ cochlea, a dramatic change given that the *Nr2f1* gene itself and more than 1 Mb of surrounding sequence were left intact. Furthermore, normalization to *Gapdh* levels revealed that *Mctp1* is expressed at much lower levels than *Nr2f1* (controls: Ct_{Mctp1}-Ct_{Gapdh}= 11.4 cycles, versus Ct_{Nr2f1}-Ct_{Gapdh}=2.47 cycles).

We next sought to confirm the functional impact of decreased gene expression by assessing NR2F1 protein distribution in the embryonic cochlea with immunofluorescence. Sections of the E16.5 cochlea of *Mctp1*$^{+/dwnd}$ control mice revealed that NR2F1 was broadly located in the cochlear floor, overlapping with SOX2 that labels the prosensory domain, but also extending more neurally (Fig. 3B). In *Mctp1*$^{dwnd/dwnd}$ mutants, however, NR2F1 antibody signal in the cochlear floor was severely reduced, and only the most abneural cells as well as non-epithelial cells outside the cochlear duct retained normal protein expression (Fig. 3B, arrowheads). By contrast, NR2F1 signals appeared unchanged in the E16.5 *Mctp1*$^{dwnd/dwnd}$ retina (Fig. 3C), and quantification of the NR2F1/SOX2 intensity ratio in both organs confirmed a significant reduction of NR2F1 in the cochlear floor but not in the retina (Fig. 3D). Overall, these results suggest that *dwnd* compromises a regulatory region located in *Mctp1* that enhances *Nr2f1* transcript and protein expression in the embryonic cochlea. This long-range regulatory region exhibits cell specificity even within the cochlear duct, probably explaining why *Mctp1*$^{dwnd/dwnd}$ mutants share the organ of Corti disorganization reported in *Nr2f1*$^{-/}$ mutants (Fig. 1B-D)(Tang et al., 2006), but not the associated postnatal lethality, for example.

3.5. Non-complementation between Mctp1^{dwnd} and *Nr2f1*$^{-}$ alleles

To formally confirm that *Mctp1*^{dwnd} is a regulatory allele of *Nr2f1*, we next asked whether the *Mctp1*^{dwnd} allele could complement a null allele of *Nr2f1* produced by the KOMP consortium (*Nr2f1*$^{tm1.1(KOMP)Mbp}$, hereafter *Nr2f1*$^{-}$). We generated transheterozygous

animals where one parental Chromosome 13 carries *Mctp1*^{dwnd} and *Nr2f1*$^{+}$ alleles and the other carries *Mctp1*$^{+}$ and *Nr2f1*$^{-}$ alleles (hereafter denoted as *Mctp1*$^{+/dwnd}$ *Nr2f1*$^{+/}$). Even though both genes were heterozygous, some of the transheterozygotes exhibited signs of vestibular dysfunction (2 out of 10 exhibited a noticeable circling behavior), and all suffered from hearing loss, with ABR thresholds recorded at 8, 16 and 32 kHz raised to similar levels as the *Mctp1*$^{dwnd/dwnd}$ mutants (Fig. 4A). The *Mctp1*$^{+/dwnd}$ *Nr2f1*$^{+/}$ transheterozygotes also shared the defective organ-scale features observed earlier in *Mctp1*$^{dwnd/dwnd}$ homozygotes: improperly separated utricle and saccule, and a shorter cochlear duct (Fig. 4B). Of note, these defects were also observed in *Nr2f1*$^{-/}$ inner ears (Fig. 4B), as expected if they originate strictly from the loss of NR2F1 function.

At the cellular level, the basal region of the cochlea in neonatal *Mctp1*$^{+/dwnd}$ *Nr2f1*$^{+/}$ transheterozygotes showed hair cell disorganization including an excess of IHCs, mirroring our results in P8 *Mctp1*$^{dwnd/dwnd}$ mutants (Fig. 5A top; compare with Fig. 1B-C). Furthermore, the apex region of the neonate cochlea in transheterozygotes exhibited extra rows of OHCs previously noted in *Mctp1*$^{dwnd/dwnd}$ mutants (Fig. 5A bottom, arrowheads; compare with Fig. 1D-E). In *Mctp1*$^{+/dwnd}$ *Nr2f1*$^{+/}$ transheterozygotes, but not in *Mctp1*$^{+/dwnd}$ *Nr2f1*$^{+/+}$ littermate controls, the utricular macula was reduced from an ovate to a trapezoid shape (Fig. 5B), and the saccular macula appeared disrupted, being often attached with the utricular macula (not shown) and the cochlear base (Fig. 5C). Altogether, these results strongly suggest that the loss of NR2F1 function in the developing *Mctp1*$^{dwnd/dwnd}$ inner ear fully accounts for physiological and morphological defects observed in both the cochlea and vestibular organs.

3.6. Targeted Mctp1 knockout mice have normal inner ear morphology and function

The phenotype of mice with *Mctp1* loss-of-function mutations has not been reported. To definitively rule out an involvement of MCTP1 dysfunction in the *dwnd/dwnd* phenotype we obtained mice with a targeted *Mctp1* knockout mutation (*Mctp1*$^{em1(IMPC)Mbp}$, hereafter *Mctp1*$^{-}$). *Mctp1*$^{-/-}$ mice appear healthy and are able to breed, with no overt behavioral or morphological abnormalities. They have normal ABR thresholds comparable to *Mctp1*$^{+/dwnd}$ control mice at one month of age (Fig. 4A), and do not exhibit the moderate circling behavior that first exposed the spontaneous *Mctp1*^{dwnd} mutation. Furthermore, paintfills at E15.5 revealed an overall normal morphology of inner ear ears in *Mctp1*$^{-/}$ mutants (Fig. 4B). Finally, the hair cell arrangement in neonatal *Mctp1*$^{-/}$ mutant cochlea was unaffected (Fig. 5A), and the shape and size of the utricular and saccular maculae were normal (Fig. 5B). Along with the lack of complementation between *Mctp1*^{dwnd} and *Nr2f1*$^{-}$ alleles, these results confirm that the loss of MCTP1 function is not the cause of the hearing loss or inner ear dysmorphology associated with the *Mctp1*^{dwnd} mutation.

4. Discussion

We provide several lines of evidence supporting our conclusion that the inner ear phenotype of *dwnd/dwnd* mutant mice is caused by the deletion of cis-regulatory sequences located within the *Mctp1* gene that enhance *Nr2f1* expression in the inner ear: (1) A deletion within the *Mctp1* gene is the causative DNA lesion underlying the abnormal inner ear phenotype of

mice homozygous for the spontaneous *dwnd* mutation. (2) MCTP1 deficiency cannot be the cause of the *Mctp1*$^{dwnd/dwnd}$ phenotype because *Mctp1*$^{-/}$ knockout mice are viable and have normal inner ear morphology and function; therefore, deletion of non-coding regulatory sequences in the *Mctp1* gene must instead be responsible. (3) The transcription factor gene *Nr2f1* is located 1.4 Mb from *Mctp1*, and the inner ear phenotype of *Nr2f1*$^{-/-}$ mice (Tang et al., 2006) is very similar to what we observed in *Mctp1*$^{dwnd/dwnd}$ mice. (4) Transcript and protein expression of *Nr2f1* is greatly reduced in inner ears of *Mctp1*$^{dwnd/dwnd}$ mice. (5) The mutant phenotype of *Mctp1*$^{dwnd/dwnd}$ *Nr2f1*$^{+/-}$ transheterozygotes is similar to that of *Nr2f1*$^{-/-}$ and *Mctp1*$^{dwnd/dwnd}$ mice, indicating genetic non-complementation of *Mctp1*^{dwnd} and *Nr2f1*$^{-}$ alleles and demonstrating a cis-regulatory effect of the *Mctp1*^{dwnd} deletion on *Nr2f1* expression. The region deleted by the *Mctp1*^{dwnd} mutation is necessary for the normal expression of *Nr2f1* during inner ear development, but the phenotypic effect of the deletion is not necessarily due to the loss of a single enhancer element. The deletion may eliminate multiple enhancer elements, or it may disrupt the 3D chromosomal conformation necessary for proper enhancer interaction with the *Nr2f1* promoter. Further experiments, including reporter assays for enhancer activity, are required to determine the underlying mechanism of this long-range, cis-regulatory region.

The *Mctp1*^{dwnd} deletion causes loss of *Nr2f1* expression in a tissue-specific manner. We found no effect of the deletion on NR2F1 expression in the retina, although expression was dramatically reduced in the inner ear (Fig. 3). *Mctp1*$^{dwnd/dwnd}$ mutants did not exhibit the lethality of *Nr2f1*$^{-/}$ mutants, indicating that their defects are restricted to organs, such as the inner ear, that are not critical to post-natal viability. The non-lethality of *Mctp1*$^{dwnd/dwnd}$ mutant mice is useful for studying the effects of *Nr2f1* deficiency specifically on inner ear function without the restrictions imposed by the perinatal lethality of *Nr2f1*$^{-/}$ knockout mice. This advantage allows for studies of *Nr2f1*-deficiency in adults, including examinations of age-related changes in inner ear histology and auditory and vestibular physiology, which are not possible in embryos or neonates.

The cis-regulatory region we discovered within the *Mctp1* gene, which is 1.4 Mb from its target gene *Nr2f1*, may represent the most distantly located mammalian enhancer thus far reported with an associated phenotypic consequence. The most distant regulatory element we could find in a search of previous publications is an enhancer associated with preaxial polydactyly that is located in intron 5 of the *Lmbr1* gene, which is 1 Mb from its target gene *Shh* (Lettice et al., 2003). Large regulatory domains of chromosomes have been shown to correspond with topologically associating domains (TADs), self-interacting physical domains that limit the extent of enhancer interactions with target genes (Symmons et al., 2014). In mammals, TAD sizes are estimated to vary from 40 kb to 3 Mb, with a median size of 185 kb (Rao et al., 2014). The 1.4 Mb distance between the *Mctp1*^{dwnd} regulatory region and its *Nr2f1* target thus falls within the expected size range of TADs.

To identify TAD boundaries for the *Mctp1*^{dwnd} regulatory region, we used the 3D Genome Browser: a web-based browser for visualizing 3D genome organization and long-range chromatin interactions (http://promoter.bx.psu.edu/hi-c/). Although the Hi-C dataset accessed from this website was generated from mouse B-lymphoblast cells (Rao et al., 2014), TAD boundaries are typically invariant across different cell types and between

species and should also apply to cells of the embryonic inner ear (Dixon et al., 2015; Jin et al., 2013; Lonfat et al., 2014). According to the Hi-C heatmap generated from this dataset, the *Mctp1*^{dwnd} deletion and the *Nr2f1* gene are located in the same TAD (Fig. 6A), supporting the possibility of a longrange physical interaction between these loci, as was deduced from our genetic analysis and expression results. The 1.55 Mb TAD containing the *Mctp1*^{dwnd} regulatory region and *Nr2f1* spans the 76,900,000-78,450,000 bp region of Chr 13 and includes four other protein-coding genes: *Pou5f2, Fam172a, 2210408I21Rik, Slf1*. Because enhancer activity is not necessarily gene specific, the *Mctp1*^{dwnd} enhancer region may also activate one of these four genes; however, inner ear expression has not been reported for any of them.

The 53 kb *Mctp1*^{dwnd} deletion spans the 76,815,703-76,868,709 bp region of Chr 13 (GRCm38), which contains exons 11-15 of *Mctp1* and surrounding intronic regions (Fig. 6B). As a first approach to identifying potential regulatoy elements within this region, we used a comparative genomic strategy because regulatory sequences, like protein-coding sequences, are often under evolutionary constraint (Visel et al., 2009). We used the ECR Browser (https://ecrbrowser.dcode.org/) to visualize evolutionarily conserved regions, comparing DNA sequence similarities of mouse with other vertebrate species (human, opossum, chicken, frog, and fish). In addition to conserved sequences corresponding to exons 11-15, five non-coding sequences located in the large intron between exons 15 and 16 are highly conserved in all of the vertebrates examined except fish (Fig. 6B) and thus could be considered candidates for enhancer elements. Homozygosity for the *Mctp1*^{dwnd} deletion reduces *Nr2f1* expression during inner ear development, which causes malformation of the utricle and saccule as well as the cochlea. Because *Nr2f1* is expressed early in the developing otic vesicle of mice (Tang et al., 2005), sequences regulating its expression are likely to be evolutionarily conserved in other vertebrate species, which share many aspects of inner ear development (Groves et al., 2012). Regulatory sequences affecting *Nr2f1* expression in inner ears of mice, however, may not be conserved in fish ears, which use vestibular sensory organs rather than a distinct auditory epithelium to respond to sound. In addition to DNA sequence conservation, potential enhancer elements also can be detected by their chromatin signatures, which require high throughput DNA sequencing often combined with chromatin immunoprecipitation (ChIP-seq) for their identification, and include transcription factor and co-factor binding sites, chromatin accessibility, histone modifications, and 3C-based methods to identify physical interactions of enhancers and promoters (Shlyueva et al., 2014). The DNA sequences selected as enhancer candidates will require functional studies to determine if they increase *Nr2f1* expression in the inner ear or if their loss diminishes expression.

The cochlear abnormalities we observed in *Mctp1*$^{dwnd/dwnd}$ mice are nearly identical to those reported in *Nr2f1*$^{-/}$ mice (Tang et al., 2006). The shorter cochlear duct (Fig. 1F,G, J) and the extra hair cells at the cochlear apex (Fig. 1E) in the inner ears of these mutant mice may be interrelated and could be the result of incomplete intercalation of post-mitotic prosensory cells during cochlear convergent extension (Driver et al., 2017). We also discovered vestibular abnormalities in inner ears of *Mctp1*$^{dwnd/dwnd}$ and *Nr2f1*$^{-/}$ mice, a finding that was not reported by Tang and colleagues (Tang et al., 2006), although a saccular abnormality is apparent in Fig. 1B of their paper. We observed that the saccule is much

reduced in size and fused with the utricle in inner ears of *Nr2f1*$^{-/}$ and *Mctp1*$^{dwnd/dwnd}$ mice and in *Mctp1*$^{+/dwnd}$ *Nr2f1*$^{+/}$ transheterozygotes (Fig. 4B), similar to the fused utriculosaccular chambers reported in inner ears of mice with mutations of other developmental control genes, including *Lmx1a* (Nichols et al., 2008; Steffes et al., 2012), *Otx1* (Morsli et al., 1999), *Hmx2* (Wang et al., 2001), and *Mycn* (N-myc) (Dominguez-Frutos et al., 2011; Kopecky et al., 2011). We also observed a large cochleosaccular duct (ductus reuniens) in the mutant inner ear (Fig. 1G) and a failed separation of the saccular macula from the cochlear base (Fig. 5C), which may be related to the disorganization of hair cells at the cochlear base (Fig. 1C, Fig. 5A). These observations are similar to, but less pronounced than, those reported for *Lmx1a*$^{-/}$ and *Mycn*$^{-/}$ mutant mice, in which the utricle, saccule, and cochlea appear continuous with one another.

In contrast to *Lmx1a*$^{-/}$, *Otx1*$^{-/}$ *Hmx2*$^{-/}$ and *Mycn*$^{-/}$ mutant mice, development of the dorsal otic epithelium appears unaffected in *Nr2f1*-deficient mice, with grossly normal endolymphatic sac and duct, semicircular canals, and ampullae (Fig. 4B). A recently proposed model of inner ear sensory patch formation (Mann et al., 2017) suggests that sensory patch boundaries are determined by the antagonistic effects of Notch signaling, which promotes *Sox2* expression and sensory domain formation, and *Lmx1a* expression, which promotes cellular commitment to a non-sensory fate. According to this model, loss of *Lmx1a* expression in boundary regions would lead to an expansion and fusion of sensory compartments. Our results suggest that *Nr2f1* may have a more limited role in the establishment of sensory patch boundaries than *Lmx1a*, being restricted to boundaries separating utricle, saccule, and cochlea.

Enhancers that affect the expression of other transcription factors and signaling molecules involved in inner ear development have been described. Loss of a long-range enhancer region located 900 kb upstream of the POU-domain transcription factor *POU3F4* gene was found to be associated with instances of X-linked deafness type 3 (de Kok et al., 1996). Multiple potential enhancers in a 1-Mb region upstream of *POU3F4* were later identified by the evolutionary conservation of their DNA sequences and their ability to enhance otic expression of a reporter gene in transgenic *Xenopus* and zebrafish (Naranjo et al., 2010). Evolutionarily conserved sequences and transgenic reporter assays have been used to identify potential inner ear enhancers of other developmentally important genes, including *Fgf10* (Ohuchi et al., 2005), *Sox9* (Bagheri-Fam et al., 2006), and *Six1* (Sato et al., 2012). More recently, the deletion of a long-range enhancer region located within the *Slc25a13* gene was shown to reduce *Dlx5* expression and disrupt inner ear development in the mouse (Johnson et al., 2018). Our discovery of a long-range regulator of *Nr2f1* expression adds to the growing list of cis-regulatory elements that determine the spatiotemporal expression patterns of key genes involved in the development of the inner ear.

Acknowledgements

We thank Melissa Berry and Vidhya Munnamalai for their helpful comments on the manuscript and the Jackson Laboratory's Reproductive Sciences Services for cryopreservation of newly developed inbred strains and importation and recovery of cryopreserved lines. This work was supported by the National Institutes of Health (NIH) grant R01 DC-0004301 (K.R.J.).B.T. is supported by NIH grant R01 DC015242. The Jackson Laboratory shared services are supported by NIH grant P30 CA-034196.

References

Armentano M, Chou SJ, Tomassy GS, Leingartner A, O'Leary DD, Studer M, 2007 COUP-TFI regulates the balance of cortical patterning between frontal/motor and sensory areas. Nature neuroscience 10, 1277–1286. [PubMed: 17828260]

Armentano M, Filosa A, Andolfr G, Studer M, 2006 COUP-TFI is required for the formation of commissural projections in the forebrain by regulating axonal growth. Development 133, 4151–4162. [PubMed: 17021036]

Bagheri-Fam S, Barrionuevo F, Dohrmann U, Gunther T, Schule R, Kemler R, Mallo M, Kanzler B, Scherer G, 2006 Long-range upstream and downstream enhancers control distinct subsets of the complex spatiotemporal Sox9 expression pattern. Developmental biology 291, 382–397. [PubMed: 16458883]

Bertacchi M, Parisot J, Studer M, 2018 The pleiotropic transcriptional regulator COUP-TFI plays multiple roles in neural development and disease Brain research.

Boettger T, Hubner CA, Maier H, Rust MB, Beck FX, Jentsch TJ, 2002 Deafness and renal tubular acidosis in mice lacking the K-Cl co-transporter Kcc4. Nature 416, 874–878. [PubMed: 11976689]

Bosch DG, Boonstra FN, Gonzaga-Jauregui C, Xu M, de Ligt J, Jhangiani S, Wiszniewski W, Muzny DM, Yntema HG, Pfundt R, Vissers LE, Spruijt L, Blokland EA, Chen CA, Baylor-Hopkins Center for Mendelian, G., Lewis RA, Tsai SY, Gibbs RA, Tsai MJ, Lupski JR, Zoghbi HY, Cremers FP, de Vries BB, Schaaf CP, 2014 NR2F1 mutations cause optic atrophy with intellectual disability. American journal of human genetics 94, 303–309. [PubMed: 24462372]

Brown KK, Alkuraya FS, Matos M, Robertson RL, Kimonis VE, Morton CC, 2009 NR2F1 deletion in a patient with a de novo paracentric inversion, inv(5)(q15q33.2), and syndromic deafness. American journal of medical genetics. Part A 149A, 931–938. [PubMed: 19353646]

Bulger M, Groudine M, 2011 Functional and mechanistic diversity of distal transcription enhancers. Cell 144, 327–339. [PubMed: 21295696]

Chen CA, Bosch DG, Cho MT, Rosenfeld JA, Shinawi M, Lewis RA, Mann J, Jayakar P, Payne K, Walsh L, Moss T, Schreiber A, Schoonveld C, Monaghan KG, Elmslie F, Douglas G, Boonstra FN, Millan F, Cremers FP, McKnight D, Richard G, Juusola J, Kendall F, Ramsey K, Anyane-Yeboa K, Malkin E, Chung WK, Niyazov D, Pascual JM, Walkiewicz M, Veluchamy V, Li C, Hisama FM, de Vries BB, Schaaf C, 2016 The expanding clinical phenotype of Bosch-Boonstra-Schaaf optic atrophy syndrome: 20 new cases and possible genotype-phenotype correlations. Genetics in medicine : official journal of the American College of Medical Genetics 18, 1143–1150. [PubMed: 26986877]

de Kok YJ, Vossenaar ER, Cremers CW, Dahl N, Laporte J, Hu LJ, Lacombe D, Fischel-Ghodsian N, Friedman RA, Parnes LS, Thorpe P, Bitner-Glindzicz M, Pander HJ, Heilbronner H, Graveline J, den Dunnen JT, Brunner HG, Ropers HH, Cremers FP, 1996 Identification of a hot spot for microdeletions in patients with X-linked deafness type 3 (DFN3) 900 kb proximal to the DFN3 gene POU3F4. Human molecular genetics 5, 1229–1235. [PubMed: 8872461]

Dixon JR, Jung I, Selvaraj S, Shen Y, Antosiewicz-Bourget JE, Lee AY, Ye Z, Kim A, Rajagopal N, Xie W, Diao Y, Liang J, Zhao H, Lobanenkov VV, Ecker JR, Thomson JA, Ren B, 2015 Chromatin architecture reorganization during stem cell differentiation. Nature 518, 331–336. [PubMed: 25693564]

Doetzlhofer A, Avraham KB, 2017 Insights into inner ear-specific gene regulation: Epigenetics and non-coding RNAs in inner ear development and regeneration. Seminars in cell & developmental biology 65, 69–79. [PubMed: 27836639]

Dominguez-Frutos E, Lopez-Hernandez I, Vendrell V, Neves J, Gallozzi M, Gutsche K, Quintana L, Sharpe J, Knoepfler PS, Eisenman RN, Trumpp A, Giraldez F, Schimmang T, 2011 N-myc Controls Proliferation, Morphogenesis, and Patterning of the Inner Ear. The Journal of neuroscience : the official journal of the Society for Neuroscience 31, 7178–7189. [PubMed: 21562282]

Driver EC, Northrop A, Kelley MW, 2017 Cell migration, intercalation and growth regulate mammalian cochlear extension. Development 144, 3766–3776. [PubMed: 28870992]

Fritzsch B, Pan N, Jahan I, Elliott KL, 2015 Inner ear development: building a spiral ganglion and an organ of Corti out of unspecified ectoderm. Cell and tissue research 361, 7–24. [PubMed: 25381571]

Furness DN, Hackney CM, 1986 High-resolution scanning-electron microscopy of stereocilia using the osmium-thiocarbohydrazide coating technique. Hearing Research 21, 243–249. [PubMed: 3522517]

Groves AK, Fekete DM, 2012 Shaping sound in space: the regulation of inner ear patterning. Development 139, 245–257. [PubMed: 22186725]

Hertzano R, Elkon R, Kurima K, Morrisson A, Chan SL, Sallin M, Biedlingmaier A, Darling DS, Griffith AJ, Eisenman DJ, Strome SE, 2011 Cell type-specific transcriptome analysis reveals a major role for Zeb1 and miR-200b in mouse inner ear morphogenesis. PLoS genetics 7, e1002309. [PubMed: 21980309]

Jin F, Li Y, Dixon JR, Selvaraj S, Ye Z, Lee AY, Yen CA, Schmitt AD, Espinoza CA, Ren B, 2013 A high-resolution map of the three-dimensional chromatin interactome in human cells. Nature 503, 290–294. [PubMed: 24141950]

Johnson KR, Gagnon LH, Tian C, Longo-Guess CM, Low BE, Wiles MV, Kiernan AE, 2018 Deletion of a Long-Range Dlx5 Enhancer Disrupts Inner Ear Development in Mice. Genetics 208, 1165–1179. [PubMed: 29301908]

Kiernan AE, 2006 The paintfill method as a tool for analyzing the three-dimensional structure of the inner ear. Brain research 1091, 270–276. [PubMed: 16600188]

Kleinjan DA, van Heyningen V, 2005 Long-range control of gene expression: emerging mechanisms and disruption in disease. American journal of human genetics 76, 8–32. [PubMed: 15549674]

Kopecky B, Santi P, Johnson S, Schmitz H, Fritzsch B, 2011 Conditional deletion of N-Myc disrupts neurosensory and non-sensory development of the ear. Developmental Dynamics 240, 1373–1390. [PubMed: 21448975]

Lettice LA, Heaney SJ, Purdie LA, Li L, de Beer P, Oostra BA, Goode D, Elgar G, Hill RE, de Graaff E, 2003 A long-range Shh enhancer regulates expression in the developing limb and fin and is associated with preaxial polydactyly. Human molecular genetics 12, 1725–1735. [PubMed: 12837695]

Livak KJ, Schmittgen TD, 2001 Analysis of relative gene expression data using real-time quantitative PCR and the 2(-Delta Delta C(T)) Method. Methods 25, 402–408. [PubMed: 11846609]

Lonfat N, Montavon T, Darbellay F, Gitto S, Duboule D, 2014 Convergent evolution of complex regulatory landscapes and pleiotropy at Hox loci. Science 346, 1004–1006. [PubMed: 25414315]

Long HK, Prescott SL, Wysocka J, 2016 Ever-Changing Landscapes: Transcriptional Enhancers in Development and Evolution. Cell 167, 1170–1187. [PubMed: 27863239]

Longo-Guess CM, Gagnon LH, Fritzsch B, Johnson KR, 2007 Targeted knockout and lacZ reporter expression of the mouse Tmhs deafness gene and characterization of the hscy-2J mutation. Mamm Genome 18, 646–656. [PubMed: 17876667]

Maass JC, Gu R, Cai T, Wan YW, Cantellano SC, Asprer JS, Zhang H, Jen HI, Edlund RK, Liu Z, Groves AK, 2016 Transcriptomic Analysis of Mouse Cochlear Supporting Cell Maturation Reveals Large-Scale Changes in Notch Responsiveness Prior to the Onset of Hearing. PloS one 11, e0167286. [PubMed: 27918591]

Mann ZF, Galvez H, Pedreno D, Chen Z, Chrysostomou E, Zak M, Kang M, Canden E, Daudet N, 2017 Shaping of inner ear sensory organs through antagonistic interactions between Notch signalling and Lmx1a. eLife 6.

McGee J, Goodyear RJ, McMillan DR, Stauffer EA, Holt JR, Locke KG, Birch DG, Legan PK, White PC, Walsh EJ, Richardson GP, 2006 The very large G-protein-coupled receptor VLGR1: a component of the ankle link complex required for the normal development of auditory hair bundles. The Journal of neuroscience : the official journal of the Society for Neuroscience 26, 6543–6553. [PubMed: 16775142]

Montemayor C, Montemayor OA, Ridgeway A, Lin F, Wheeler DA, Pletcher SD, Pereira FA, 2010 Genome-wide analysis of binding sites and direct target genes of the orphan nuclear receptor NR2F1/COUP-TFI. PloS one 5, e8910. [PubMed: 20111703]

Morsli H, Tuorto F, Choo D, Postiglione MP, Simeone A, Wu DK, 1999 Otxl and Otx2 activities are required for the normal development of the mouse inner ear. Development 126, 2335–2343. [PubMed: 10225993]

Naranjo S, Voesenek K, de la Calle-Mustienes E, Robert-Moreno A, Kokotas H, Grigoriadou M, Economides J, Van Camp G, Hilgert N, Moreno F, Alsina B, Petersen MB, Kremer H, Gomez-Skarmeta JL, 2010 Multiple enhancers located in a 1Mb region upstream of POU3F4 promote expression during inner ear development and may be required for hearing. Human genetics 128, 411–419. [PubMed: 20668882]

Nichols DH, Pauley S, Jahan I, Beisel KW, Millen KJ, Fritzsch B, 2008 Lmx1a is required for segregation of sensory epithelia and normal ear histogenesis and morphogenesis. Cell and tissue research 334, 339–358. [PubMed: 18985389]

Oberdick J WJ, Lewin A, Smeyne RJ, 1994 Transgenic expression to monitor dynamic organization of neuronal development: use of the Escherichia coli lacZ gene product, □-galactosidase. Neuroprotocols 5, 54–62.

Ohuchi H, Yasue A, Ono K, Sasaoka S, Tomonari S, Takagi A, Itakura M, Moriyama K, Noji S, Nohno T, 2005 Identification of cis-element regulating expression of the mouse Fgf10 gene during inner ear development. Developmental dynamics : an official publication of the American Association of Anatomists 233, 177–187. [PubMed: 15765517]

Ong CT, Corces VG, 2011 Enhancer function: new insights into the regulation of tissue-specific gene expression. Nature reviews. Genetics 12, 283–293.

Pangrsic T, Reisinger E, Moser T, 2012 Otoferlin: a multi-C2 domain protein essential for hearing. Trends in neurosciences 35, 671–680. [PubMed: 22959777]

Pereira FA, Tsai MJ, Tsai SY, 2000 COUP-TF orphan nuclear receptors in development and differentiation. Cellular and molecular life sciences : CMLS 57, 1388–1398. [PubMed: 11078018]

Qiu Y, Pereira FA, DeMayo FJ, Lydon JP, Tsai SY, Tsai MJ, 1997 Null mutation of mCOUP-TFI results in defects in morphogenesis of the glossopharyngeal ganglion, axonal projection, and arborization. Genes & development 11, 1925–1937. [PubMed: 9271116]

Rao SS, Huntley MH, Durand NC, Stamenova EK, Bochkov ID, Robinson JT, Sanborn AL, Machol I, Omer AD, Lander ES, Aiden EL, 2014 A 3D map of the human genome at kilobase resolution reveals principles of chromatin looping. Cell 159, 1665–1680. [PubMed: 25497547]

Sato S, Ikeda K, Shioi G, Nakao K, Yajima H, Kawakami K, 2012 Regulation of Six1 expression by evolutionarily conserved enhancers in tetrapods. Developmental biology 368, 95–108. [PubMed: 22659139]

Shin OH, Han W, Wang Y, Sudhof TC, 2005 Evolutionarily conserved multiple C2 domain proteins with two transmembrane regions (MCTPs) and unusual Ca2+ binding properties. J Biol Chem 280, 1641–1651. [PubMed: 15528213]

Shlyueva D, Stampfel G, Stark A, 2014 Transcriptional enhancers: from properties to genome-wide predictions. Nature reviews. Genetics 15, 272–286.

Spitz F, 2016 Gene regulation at a distance: From remote enhancers to 3D regulatory ensembles. Seminars in cell & developmental biology 57, 57–67. [PubMed: 27364700]

Steffes G, Lorente-Canovas B, Pearson S, Brooker RH, Spiden S, Kiernan AE, Guenet JL, Steel KP, 2012 Mutanlallemand (mtl) and Belly Spot and Deafness (bsd) are two new mutations of Lmx1a causing severe cochlear and vestibular defects. PloS one 7, e51065. [PubMed: 23226461]

Symmons O, Uslu VV, Tsujimura T, Ruf S, Nassari S, Schwarzer W, Ettwiller L, Spitz F, 2014 Functional and topological characteristics of mammalian regulatory domains. Genome research 24, 390–400. [PubMed: 24398455]

Tang LS, Alger HM, Lin F, Pereira FA, 2005 Dynamic expression of COUP-TFI and COUP-TFII during development and functional maturation of the mouse inner ear. Gene expression patterns : GEP 5, 587–592. [PubMed: 15907456]

Tang LS, Alger HM, Pereira FA, 2006 COUP-TFI controls Notch regulation of hair cell and support cell differentiation. Development 133, 3683–3693. [PubMed: 16914494]

Tian C, Gagnon LH, Longo-Guess C, Korstanje R, Sheehan SM, Ohlemiller KK, Schrader AD, Lett JM, Johnson KR, 2017 Hearing loss without overt metabolic acidosis in ATP6V1B1 deficient

MRL mice, a new genetic model for non-syndromic deafness with enlarged vestibular aqueducts. Human molecular genetics 26, 3722–3735. [PubMed: 28934385]

Truett GE, Heeger P, Mynatt RL, Truett AA, Walker JA, Warman ML, 2000 Preparation of PCR-quality mouse genomic DNA with hot sodium hydroxide and tris (HotSHOT). Biotechniques 29, 52, 54. [PubMed: 10907076]

Visel A, Rubin EM, Pennacchio LA, 2009 Genomic views of distant-acting enhancers. Nature 461, 199–205. [PubMed: 19741700]

Wang W, Chan EK, Baron S, Van de Water T, Lufkin T, 2001 Hmx2 homeobox gene control of murine vestibular morphogenesis. Development 128, 5017–5029. [PubMed: 11748138]

Wu DK, Kelley MW, 2012 Molecular mechanisms of inner ear development. Cold Spring Harbor perspectives in biology 4, a008409. [PubMed: 22855724]

Yamaguchi H, Zhou C, Lin SC, Durand B, Tsai SY, Tsai MJ, 2004 The nuclear orphan receptor COUP-TFI is important for differentiation of oligodendrocytes. Developmental biology 266, 238–251. [PubMed: 14738874]

Zhang G, Shi J, Zhu S, Lan Y, Xu L, Yuan H, Liao G, Liu X, Zhang Y, Xiao Y, Li X, 2018 DiseaseEnhancer: a resource of human disease-associated enhancer catalog. Nucleic acids research 46, D78–D84. [PubMed: 29059320]

Zhou C, Qiu Y, Pereira FA, Crair MC, Tsai SY, Tsai MJ, 1999 The nuclear orphan receptor COUP-TFI is required for differentiation of subplate neurons and guidance of thalamocortical axons. Neuron 24, 847–859. [PubMed: 10624948]

Zhou C, Tsai SY, Tsai MJ, 2001 COUP-TFI: an intrinsic factor for early regionalization of the neocortex. Genes & development 15, 2054–2059. [PubMed: 11511537]

Highlights:

- The recessive *dwnd* mutation is a spontaneous deletion in the mouse *Mctp1* gene first identified by the circling behavior of homozygotes.
- Homozygosity for *dwnd* also causes hearing loss and inner ear structural defects.
- *Nr2f1* downregulation, and not *Mctp1* inactivation, accounts for the aberrant inner ear phenotype of $Mctp1^{dwnd/dwnd}$ mutants.
- The $Mctp1^{dwnd}$ deletion abrogates a cis-regulatory region located 1.4 Mb away but essential for *Nr2f1* expression in the embryonic inner ear.
- In addition to previously reported cochlear defects, *Nr2f1*-deficient mice exhibit vestibular abnormalities, including a fusion of the utricle and saccule and an enlarged cochleosaccular duct.

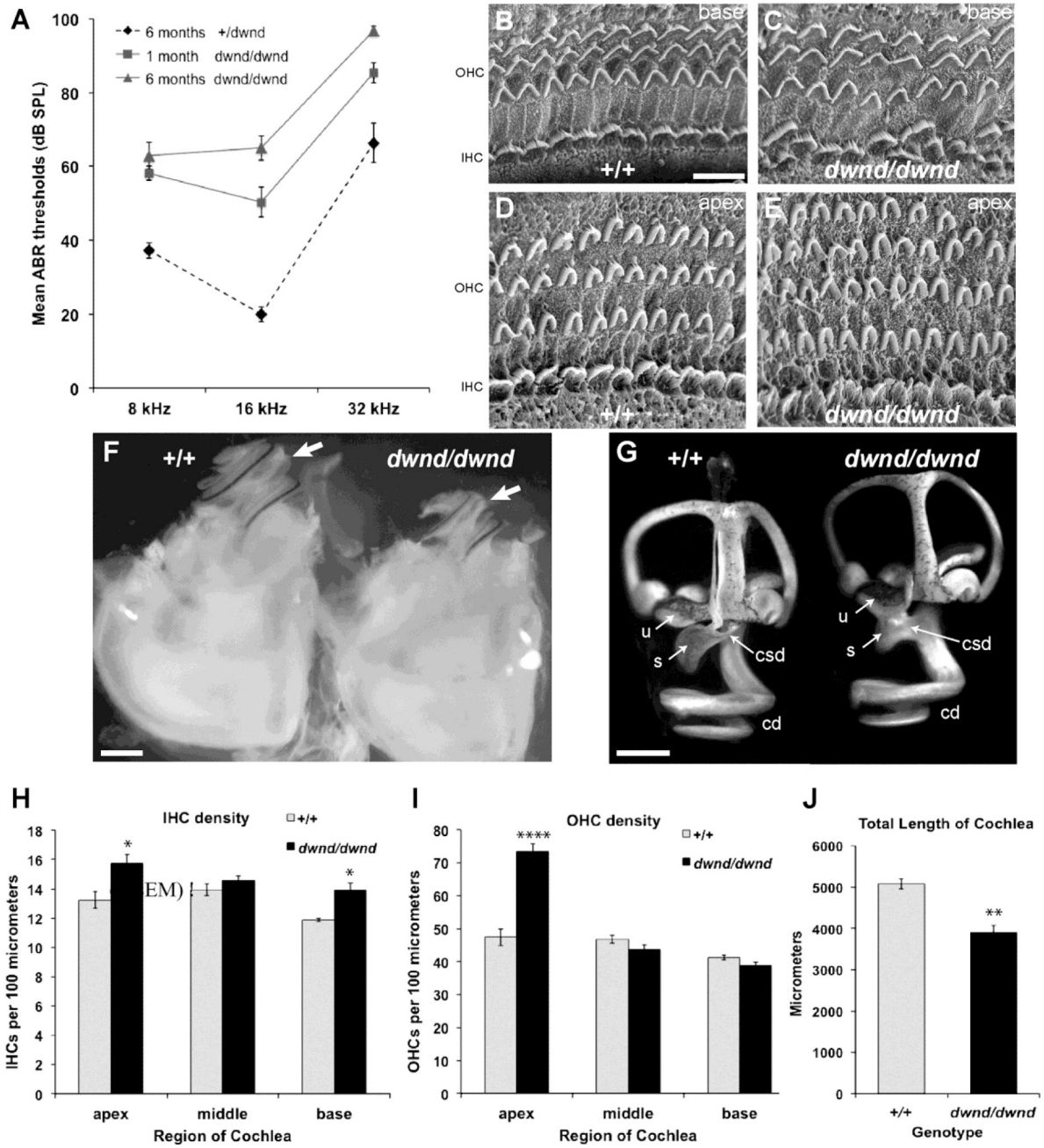

Figure 1. Auditory dysfunction and inner ear abnormalities of *dwnd/dwnd* mice.

(A) Mice homozygous for the *dwnd* mutation are hearing impaired. Means (± SEM) of ABR thresholds of 16 *dwnd/dwnd* mice tested at one month of age and 12 tested at six months of age were compared with those of 7 +/*dwnd* control mice tested at six months of age for 8, 16, and 32 kHz test stimuli. Thresholds of mutant mice were about 20-30 dB higher than those of controls at one month of age and about 25-45 dB higher at six months of age. **(B-E)** Cochleae of *dwnd/dwnd* mice have regions with supernumerary hair cells. SEM images of organ of Corti surface preparations from cochleae of P8 mice show extra inner hair cells (IHC) at the cochlear base (**C**) and an extra row of outer hair cells (OHC) at the apex (**E**) of

dwnd/dwnd mice as compared with corresponding +/+ controls (**B, D**). Scale bar for B-E (shown in B), 10 μm. (**F**) The overall size of the cochlea (indicated by arrows) in *dwnd/dwnd* mice is smaller than that of +/+ controls. Dissected inner ears of adult mice that also carry a copy of an *Lhfpl5-LacZ* reporter gene were cleared and the cochlear spiral exposed, showing rows of hair cells stained with LacZ (see Methods). Scale bar, 0.5 mm. (**G**) Inner ear paintfills of P1 (newborn) mice. In addition to a shorter cochlear duct (cd), the *dwnd/dwnd* inner ear has a smaller saccule (s) that is not separated from the utricle (u) and a much larger cochleosaccular duct (csd) than the +/+ control. Scale bar, 0.5 mm. (**H-J**) Cochlear lengths and hair cell densities in *dwnd/dwnd* and control mice. The density of inner hair cells near the apex and near the base of the cochlea is greater in *dwnd/dwnd* mutants than controls (**H**), and the density of outer hair cells near the cochlear apex is much greater in *dwnd/dwnd* mice than controls (**I**). Although hair cell densities are greater, the length of the cochlear duct is shorter in *dwnd/dwnd* mutants than controls (**J**), suggesting that total hair cell counts are similar. Means and standard error bars are shown for the average measurements of individual mice of each genotype (ten ears of +/+ mice and nine ears of *dwnd/dwnd* mice). Statistical significance of mean differences was determined using a student's t-test. * $p<0.01$; **** $p<0.0001$.

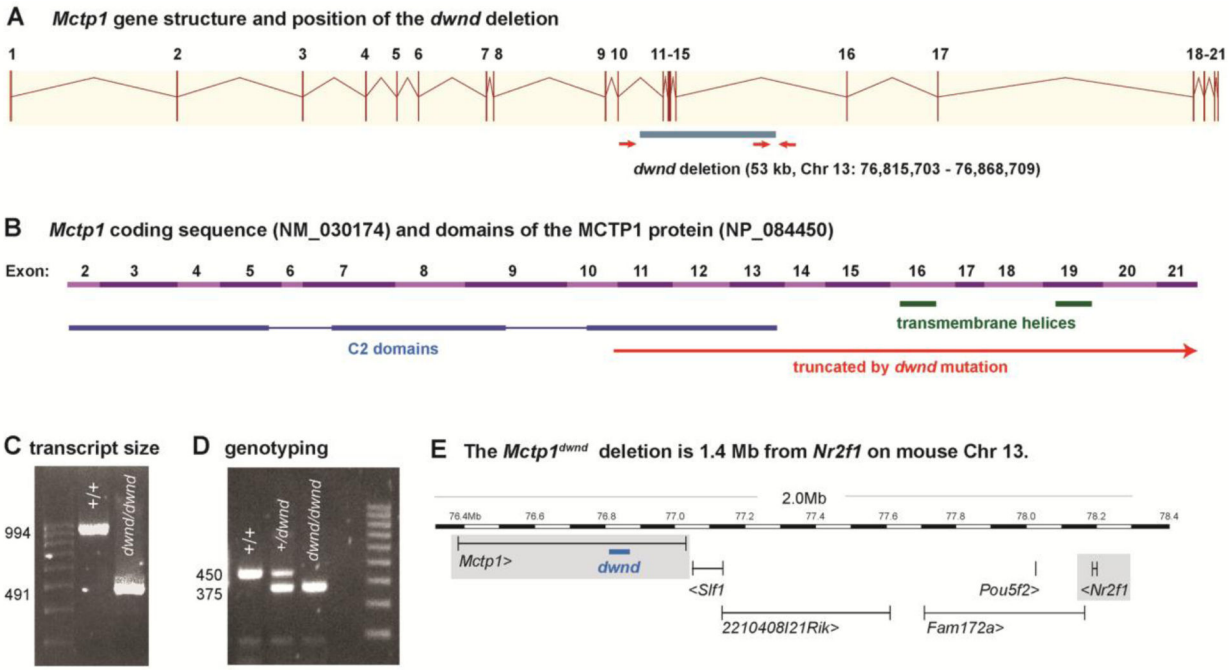

Figure 2. The *dwnd* mutation of the *Mctp1* gene.

(A) The structure of the *Mctp1* gene is shown as numbered vertical lines representing exons and horizontal connecting lines representing introns. The *dwnd* mutation (represented by the blue-gray bar beneath the gene diagram) is a 53 kb intragenic deletion of *Mctp1*, which includes exons 11-15 and adjoining intronic regions. The red arrows indicate positions and directions of PCR primers designed to distinguish wildtype and *dwnd* alleles. **(B)** Alternating pink and purple line segments indicate the exon-encoded regions of the protein-coding portion of the *Mctp1* transcript, with corresponding protein domains shown below. The out-of-frame *dwnd* mutation is expected to create a premature stop codon and truncate the protein after exon 10, thereby eliminating the third C2 domain and the two transmembrane helices of the encoded MCTP1 protein, as shown by the horizontal red arrow. **(C)** The *dwnd* mutation in the *Mctp1* gene was first identified by RT-PCR. Amplification of cDNA from brain tissue of mutant mice with primers in exons 9 and 17 of the *Mctp1* transcript (NM_03174) produced a product that was 503 bp smaller than that of the +/+ control, corresponding to the loss of exons 11-15. **(D)** A simple PCR assay of genomic DNA was designed to genotype mice with the *dwnd* mutation. The PCR assay (using three primers positioned as shown in A) amplifies a 450 bp product from the wildtype + allele and a 375 bp product from the mutant *dwnd* allele. Genotypes can be determined by the presence or absence of these PCR products as shown in the gel image for +/+, +/*dwnd*, and *dwnd/dwnd* individuals. **(E)** The site of the $Mctp1^{dwnd}$ deletion at the 76.8 Mb position on mouse Chromosome 13 is 1.4 Mb from the *Nr2f1* gene at the 78.2 Mb position. The *Mctp1* (21 exons) and *Nr2f1* (3 exons) genes are shaded in gray, and a blue horizontal bar beneath the *Mctp1* gene designates the position and extent of the *dwnd* deletion. Genome coordinates are shown above. Panels A, B, and E were derived from the mouse Ensembl Genome Browser (GRCm38).

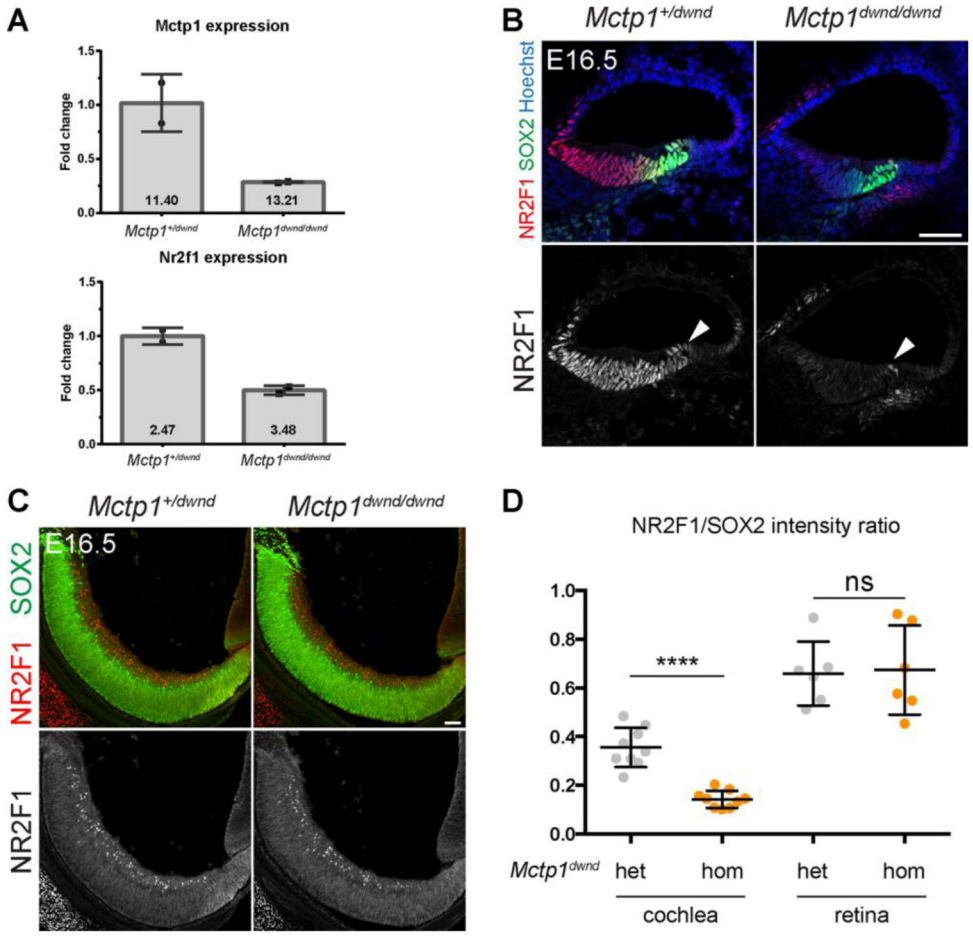

Figure 3. *Nr2f1* transcript and protein downregulation in *Mctp1*^{dwnd} cochlea.

(A) RT-qPCR on E16.5 cochleae pooled by genotype. *Mctp1* expression is reduced by about 75% in *Mctp*$^{dwnd/dwnd}$ mutants, and *Nr2f1* expression is reduced by about 50%. Data points represent samples pooled by genotype for each of two litters collected (see Methods). Numbers inside the bars indicate the average ΔCT = Ct_{target} - Ct_{Gapdh}, and reveal that *Nr2f1* is much more abundantly expressed at E16.5 than is *Mctp1*. **(B-C)** E16.5 immunodetection of NRF1 (red) and SOX2 (green) proteins in cochlear cryosections in the basal turn (**B**) and in half-retina at the optic nerve (**C**). In the cochlear floor (**B**), NR2F1 protein is enriched at much lower levels in *Mctp1*$^{dwnd/dwnd}$ compared to heterozygote controls, whereas SOX2 is comparable. Arrowheads point to abneural cells in the sensory domain that interestingly appear to retain normal NR2F1 protein in homozygotes. In the retina (**C**), NR2F1 is by contrast enriched in a comparable manner in *Mctp1*$^{dwnd/dwnd}$ and controls. (**D**) Quantification of the immunostaining intensity ratio between colocalized NR2F1 and SOX2 proteins in the E16.5 cochlea and retina. Using SOX2 as an internal control, NR2F1 is significantly downregulated in the cochlea but not in the retina. Each point represents one section (10 cochlea or 6 retina sections per genotype), two animals represented per genotype; average +/− SD; unpaired t-test with Welch's correction, ns, not significant; **** $p<0.0001$). Scale bars 50 μm.

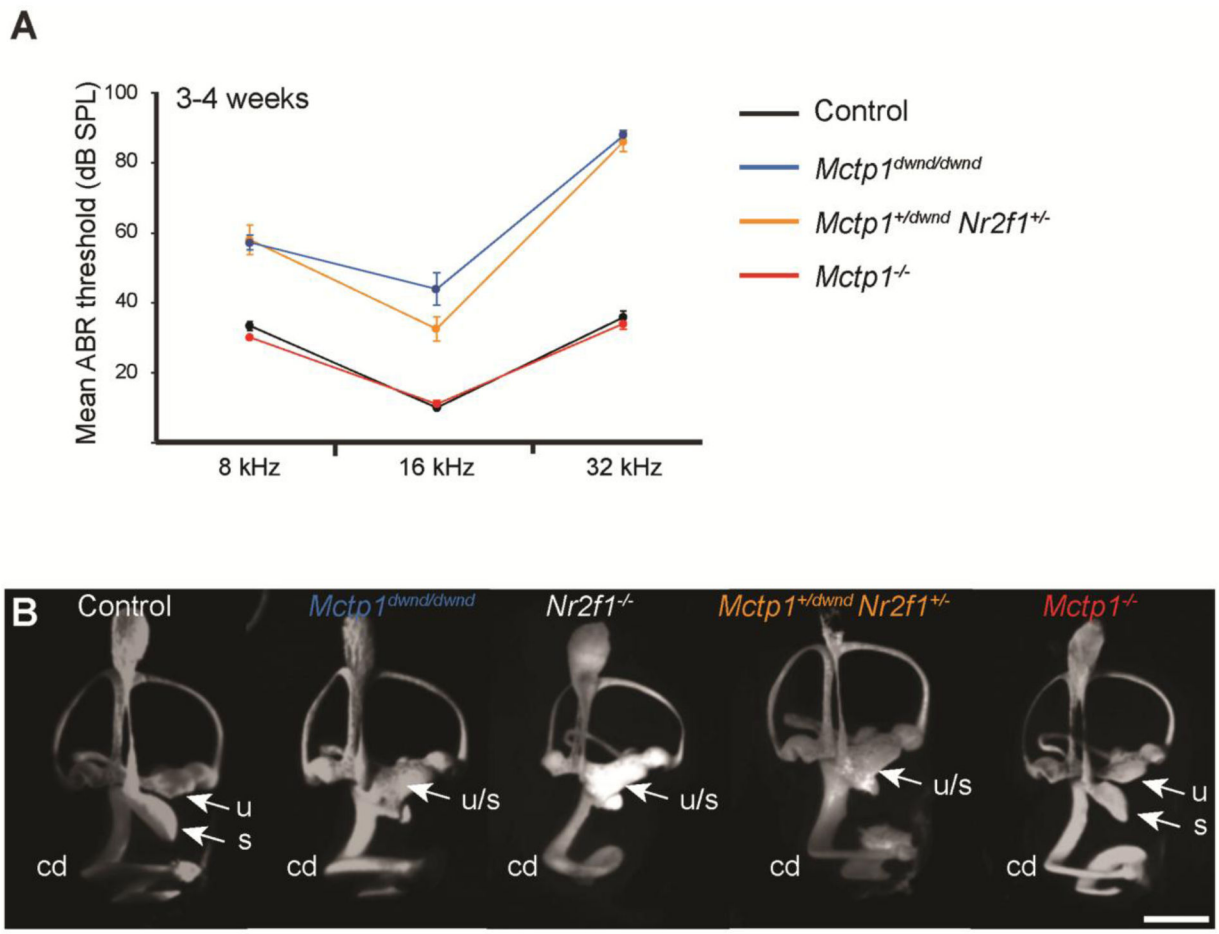

Figure 4. Hearing thresholds and inner ear paintfills of *Mctp1*$^{dwnd/dmid}$, *Mctp1*$^{-/-}$, *Nr2f1*$^{-/-}$ and *Mctp1*$^{+/dwnd}$ *Nr2f1*$^{+/-}$ mice.

(A) *Mctp1*$^{dwnd/dwnd}$ mice and *Mctp1*$^{+/dwnd}$ *Nr2f1*$^{+/-}$ transheterozygotes are hearing impaired. Mean (± SEM) ABR thresholds of 11 *Mctp1*$^{dwnd/dwnd}$ mice and 10 *Mctp1*$^{+/dwnd}$ *Nr2f1*$^{+/-}$ transheterozygotes and 12 *Mctp1*$^{-/-}$ mice tested at one month of age were compared with those of 12 age-matched *Mctp1*$^{+/dwnd}$ heterozygous control mice for 8, 16, and 32 kHz test stimuli Thresholds of *Mctp1*$^{dwnd/dwnd}$ and *Mctp1*$^{+/dwnd}$ *Nr2f1*$^{+/-}$ mice are not statistically significantly different from each other but are about 25-50 dB higher than those of *Mctp1*$^{+/dwnd}$ control mice. In contrast, thresholds of *Mctp1*$^{-/-}$ mice are not statistically significantly different than those of control mice. *Nr2f1*$^{-/-}$ mice are not included in the hearing test comparisons because they die after birth. **(B)** Inner ear paintfills of E15.5 embryos clearly show the fusion of the utricle (u) and saccule (s) in inner ears of *Mctp1*$^{dwnd/dwnd}$, *Nr2f1*$^{-/-}$, and *Mctp1*$^{+/-}$ *Nr2f1*$^{+/-}$ mice (u/s) but not in the *Mctp1*$^{-/-}$ mice. A smaller and shortened cochlear duct (cd) can also be seen in inner ears of the three mutant strains with u/s fusions. Scale bar, 0.5 mm.

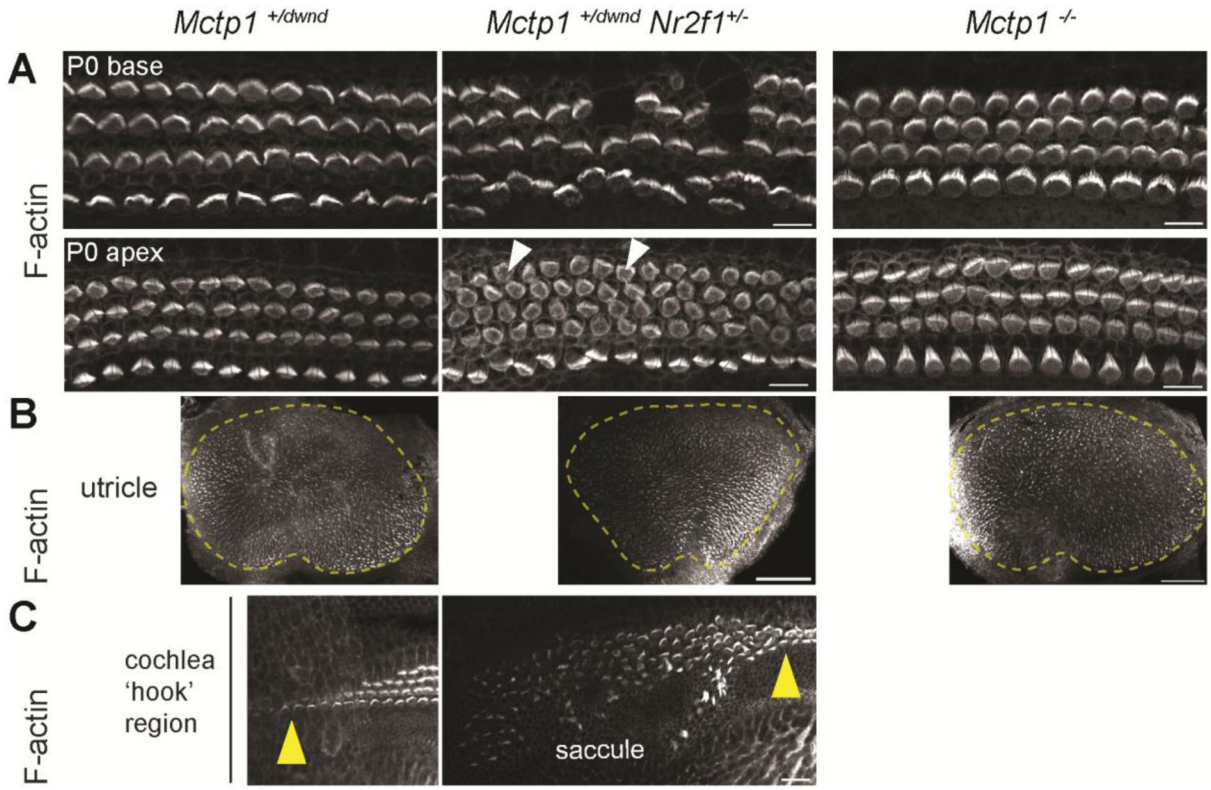

Figure 5. Hair cell patterning in inner ears of *Mctp1*$^{dwnd/dwnd}$, *Mctp1*$^{+/dwnd}$ *Nr2f1*$^{+/-}$, and *Mctp1*$^{-/-}$ mice.

All panels show phalloidin-stained flat mounts. **(A)** P0 organ of Corti for the genotypes and positions indicated. *Mctp1*$^{+/dwnd}$ *Nr2f1*$^{+/}$ transheterozygotes show hair cell disorganization at the base (top) and extra OHC rows at the apex (bottom, arrowheads), as seen in the *Mctp1*$^{dwnd/dwnd}$ mutants (see Fig. 1B-E). In contrast, hair cell organization in targeted *Mctp1* mutants (*Mctp1*$^{-/-}$) looks normal. **(B)** P0 utricle with the sensory region (macula) outlined. Transheterozygotes show a dysmorphic macula, unlike *Mctp1*$^{-/-}$ mutants. **(C)** P0 cochlear base showing failed separation of the sensory epithelia of the cochlea and the saccular macula in transheterozygotes. Arrowheads indicate the basal most position of the organ of Corti. *Mctp1*$^{-/-}$ have a normal saccule (not shown). *Mctp1*$^{+/dwnd}$ is used as control. Scale bars, 10 μm (A), 100 μm (B) and 20 μm (C).

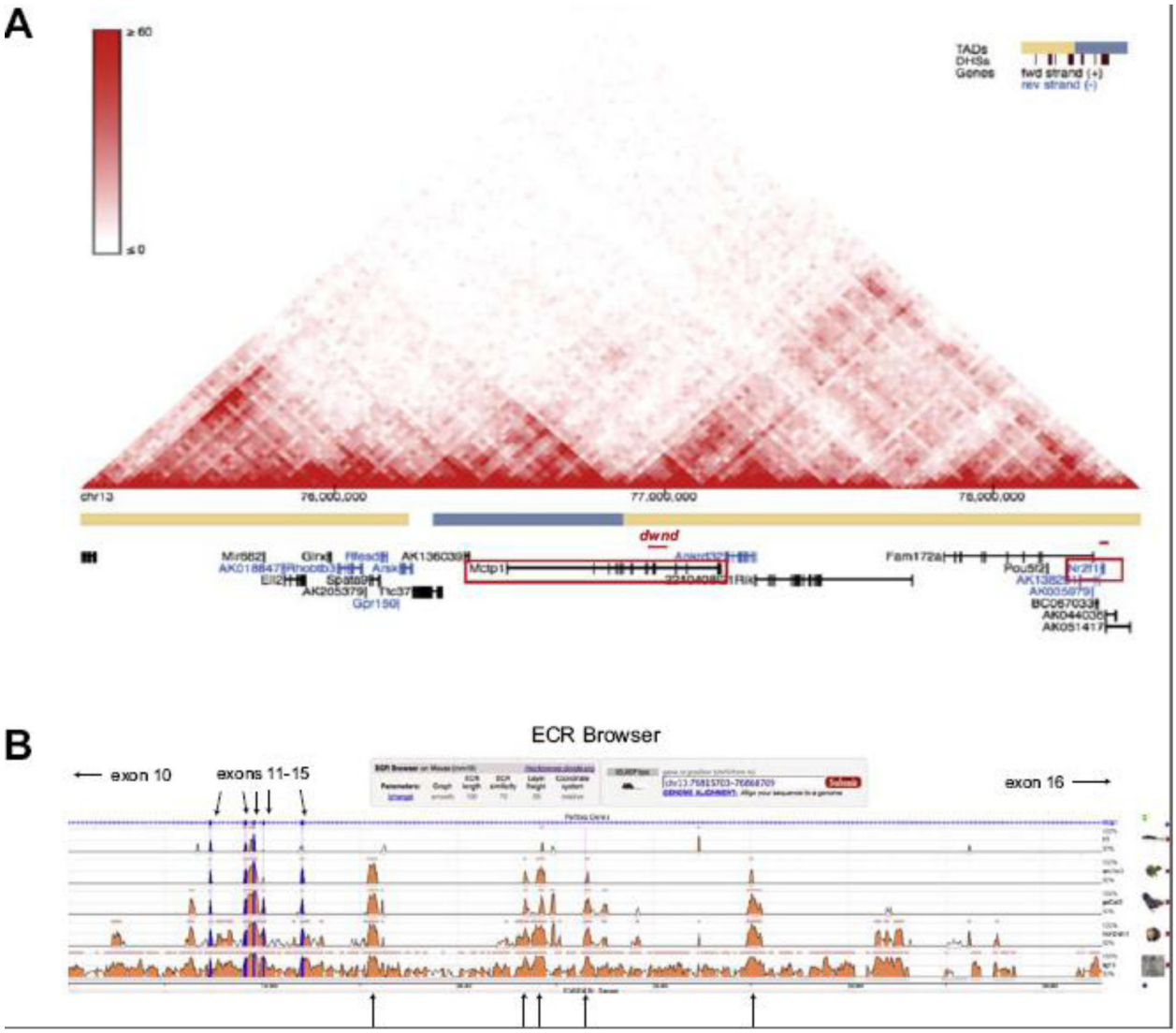

Figure 6. Supplementary information accessed from public database browsers.

(A) *Mctp1*^{dwnd} and *Nr2f1* are in the same TAD. The *Mctp1*^{dwnd} deletion and the *Nr2f1* gene (shown by horizontal red bars above the gene diagrams enclosed by red rectangles) are located in the same topologically associating domain (TAD), supporting the possibility of long-range chromatin interactions. The Hi-C heatmap was obtained from the 3D Genome Browser: a web-based browser for visualizing 3D genome organization and long-range chromatin interactions (http://promoter.bx.psu.edu/hi-c/). Although the heatmap shown in this figure was generated from Hi-C analysis of mouse B-lymphoblast cells (Rao et al., 2014), TADs are relatively constant between different cell types and are highly conserved across species, and so should be similar in the mouse embryonic inner ear. **(B)** Conserved DNA sequences suggest possible enhancer elements in the *Mctp1*^{dwnd} deleted region. Multiple phylogenetically conserved DNA sequences are present in the 53 kb *Mctp1*^{dwnd} deletion (Chr13: 76,815,703-76,868,709; GRCm38). The ECR Browser (https://ecrbrowser.dcode.org/) was used to compare DNA sequence similarities of mouse with other vertebrate species (human, opossum, chicken, frog, and fish). In addition to the sequences

corresponding to exons 11-15 (indicated by downward pointing arrows), five non-coding sequences are highly conserved in all of the vertebrates except fish (indicated by upward pointing arrows).